

TITLE:

Seizure-onset mapping based on time-varying multivariate functional connectivity analysis of high-dimensional intracranial EEG: a Kalman filter approach.

Authors: Octavian V. Lie<sup>1,\*</sup>, Pieter van Mierlo<sup>2,3\*</sup>

\* The authors have contributed equally to this work.

Affiliations: <sup>1</sup>Department of Neurology, University of Texas Health Science Center at San Antonio, San Antonio, TX 78229, USA

<sup>2</sup>Functional Brain Mapping Laboratory, EEG and Epilepsy Unit, University of Geneva, Geneva, Switzerland

<sup>3</sup>Medical Image and Signal Processing Group, Ghent University – iMinds Medical IT Department, Ghent, Belgium

Corresponding Author: Octavian V. Lie

8300 Floyd Curl Drive. MSC: 7883

San Antonio, TX 78229-3900

Phone: 210-450-0509

Fax: 210-562-9366

Email: [lie@uthscsa.edu](mailto:lie@uthscsa.edu)

## ABSTRACT

The visual interpretation of intracranial EEG (iEEG) is used clinically to map the regions of seizure onset targeted for resection during epilepsy surgery. Still, visual iEEG analysis is labor-intensive and biased due to interpreter dependency. Multivariate parametric functional-connectivity measures using adaptive autoregressive (AR) modeling of the iEEG signal based on the Kalman filter algorithm have been used successfully to localize the electrographic seizure onsets. Due to their high computational cost, these methods have been applied to a limited number of iEEG time-series (<60). The aim of this study was to test two Kalman filter implementations, a well-known multivariate adaptive AR model (Arnold et al. 1998) and a simplified, computationally efficient derivation of it, for their potential application to connectivity analysis of high-dimensional (up to 192 channels) iEEG data. When used together with a multivariate connectivity estimator, the partial directed coherence, the two AR models were compared in seizure simulations for their ability to reconstitute the designed seizure signal connections from noisy data. Next, the onset of a 113-channel iEEG seizure recorded in a patient rendered seizure-free after surgery was estimated with the out-degree, a graph-theory index of outward directed connectivity. Simulation results indicated high mapping accuracy for the two models in the presence of low-to-moderate noise cross-correlation. Accordingly, both AR models correctly mapped the real seizure onset to the resection volume. This study supports the possibility of conducting fully data-driven multivariate connectivity estimations on high-dimensional iEEG datasets using the Kalman filter approach.

Keywords: intracranial EEG; seizure; epilepsy surgery; functional connectivity; autoregressive modeling; Kalman filter

## ACKNOWLEDGMENT

This project has received funding from the University of Texas Health Science Center at San Antonio SOM/IIMS grant no. 158580; and the European Union's Horizon 2020 research and innovation program under the Marie Skłodowska-Curie grant agreement No 660230.

## INTRODUCTION

For patients with focal epilepsy resistant to medical therapy, epilepsy surgery can lead to a life free of seizures. In planning for resection, one must correctly identify the brain region(s) where seizures arise (Rosenow and Lüders 2000). To this end, a presurgical evaluation routine is applied, initially consisting of noninvasive studies (structural MRI, scalp EEG, and functional neuroimaging studies). In complex surgical cases, these noninvasive studies inform where electrodes are placed on the cortex or inside the brain parenchyma to record intracranial EEG (iEEG). Despite the use of visual iEEG analysis, the current gold standard for mapping the seizure onset, only 33-68% of the patients undergoing resective surgery become seizure-free (Bulacio et al. 2012; Carrette et al. 2010). For the rest, approximately half of the poor seizure outcomes are thought to be due to incorrect preoperative seizure-onset localization (Bulacio et al. 2012).

A growing body of research has applied quantitative methods studying connectivity among brain regions in order to complement the standard iEEG analysis of epileptic activity (Andrzejak et al. 2014; van Mierlo et al. 2014). These efforts have contributed to a better understanding of epilepsy as a network-based disorder (Yaffe et al. 2015), and have driven new research fields such as virtual epilepsy surgery (Sinha et al. 2014). Methods based on functional connectivity model the statistical dependencies among time-series in the time or frequency domain into spatially resolved connectivity matrices. If analyzed over time to characterize seizures, these matrices reflect the dynamic interactions among the iEEG time-series during the course of the seizure, and are used to derive network graphs mapping the seizure onset and propagation. Among an extensive array of functional-connectivity measures, multivariate, linear, frequency-domain measures based on the concept of Granger causality (Granger, 1969) have shown promising results in localizing the regions of seizure onset (Korzeniewska et al. 2014; van Mierlo et al. 2011, 2013; Varotto et al. 2010, 2012; Wilke et al. 2008). Briefly, it is said that one time-series Granger-causes a second if its past values help predict the second better than the past values of the second alone. Accordingly, Granger-causality measures use autoregressive (AR) models to denoise and parametrize the iEEG ‘seizure signal’ with a set of AR coefficients encoding the linear contribution of its recent past (Schlögl 2000).

To address signal nonstationarities in the time domain typical of seizures, two basic AR model techniques have been used. In the segmentation approach, the iEEG data is divided in short windows of relative signal stationarity shifting in time, and the AR coefficients are estimated for each segment (Ding et al. 2000; Korzeniewska et al. 2014). In an alternative approach, AR coefficients are allowed to vary in time and can be estimated adaptively. Among several existing adaptive time-varying AR algorithms, random-walk models based on Kalman filter (Kalman 1960; Kalman and Bucy 1961) have shown superior performance in the univariate (Schlögl 2000) and multivariate (Arnold et al. 1998) cases, and have been used successfully to map seizure-onset regions (van Mierlo et al. 2011, 2013; Wilke et al. 2008).

The application of the Kalman-filter AR models to high-dimensional data requires a significant computational effort (Arnold et al. 1998; Blinowska 2011). As a result, these models have been generally applied to a limited number of iEEG channels/time-series (up to 60, Toppi et al. 2012), often handpicked based on preferential involvement in the process under study (‘signal-enriched’ channels) or other data reduction criteria (Milde et al. 2010). This approach suffers from a hidden-source problem since multivariate connectivity methods assume that all relevant signals are analyzed (Schlögl and Supp 2006). Moreover, data reduction amplifies the inherent limitation of iEEG recordings in sampling cerebral activity when used for mapping certain neurophysiological events. For example, seizure-onset localization by iEEG requires at times an extensive implantation of hundreds of intracranial electrode contacts due to the narrow, near-field view of intracranial recordings.

The aim of this study is to evaluate a well-published multivariate adaptive AR model based on Kalman filter (Arnold et al. 1998), and a computationally efficient AR model derived from it, for their potential application to high-dimensional (up to 192) time-series. The two AR methods differ in how they model the measurement or observational noise that may contaminate the recordings. This paper is organized as follows: (1) The theoretical framework of the two AR models is exposed. (2) The AR coefficients resulting from the application of each model to simulated seizures are used to estimate the underlying connectivity structures in the presences of various degrees of correlated noise. Thereby, the relative performance of the two models in characterizing the ground-truth seizure networks is evaluated. (3) The onset of an iEEG seizure recorded in a surgical patient is identified by mapping the time-variant connections based on the two AR models. The resulting seizure-onset estimates are compared based on colocalization with the resection volume, and the correlation of the dynamic connectivity maps based on the two models is determined. Next, the effect of AR modelling of low- and high-density seizure datasets is analyzed. (4) The computational cost of the two models is evaluated. (5) Finally, the results and significance of the Kalman filter approach herein are discussed.

## METHODS

### Autoregressive modeling

In its scalar form, an AR model of order  $p$  is given by

	$y(n) = \sum_{k=1}^p a_k y(n-k) + e(n)$	1
--	---	---

where  $y(n)$  is the  $n^{\text{th}}$  observation of a signal or time-series,  $a_1 \dots a_p$  are AR coefficients specifying the linear contribution of the previous  $p$  signal observations, and  $e(n)$  is assumed a series of independent, normally distributed variables uncorrelated over time (zero autocorrelation at lag  $i, i > 0$ ), with zero mean and variance  $\sigma^2$  (i.d.  $\sim N(0, \sigma^2)$ ). In effect,  $e(n)$  is a white-noise process reflecting the uncertainty in predicting the signal of interest recursively (prediction error).

For multivariate time-series, the vector representation of a time-varying AR process is

	$\mathbf{y}(n) = \sum_{k=1}^p \mathbf{A}_k(n) \mathbf{y}(n-k) + \mathbf{e}(n)$	2
--	--	---

where  $\mathbf{y}(n) = (y_1(n), y_2(n) \dots y_s(n))^T$  for  $s$  signals/channels,  $\mathbf{A}_k$  is the  $s \times s$  coefficient matrix at delay  $k$ , and  $\mathbf{e}(n) = (e_1(n), e_2(n) \dots e_s(n))^T$ .

The application of the Kalman algorithm to estimate the AR coefficients makes use of the state-space model of the AR process, which consists of a system or state equation,

	$\mathbf{x}(n+1) = \mathbf{F}(n+1, n) \mathbf{x}(n) + \mathbf{v}_1(n)$	3
--	--	---

and an observation or measurement equation,

	$\mathbf{y}(n) = \mathbf{H}(n) \mathbf{x}(n) + \mathbf{v}_2(n)$	4
--	---	---

Equation 3 relates the state vector  $\mathbf{x}(n)$  of AR coefficients,

	$\mathbf{x}(n) = (a_{111}(n), \dots, a_{1s1}(n), a_{112}(n), \dots, a_{1s2}(n), \dots, a_{1sp}(n), a_{211}(n), \dots, a_{ssp}(n))^T$	5
--	--	---

to the state at time  $n+1$  by defining the state transition matrix,  $\mathbf{F}(n+1, n)$ , and the system white-noise process  $\mathbf{v}_1(n) = N(\mathbf{0}, \mathbf{Q}_1(n))$ . In equation 4,  $\mathbf{H}(n)$  is called the measurement matrix, and relates the current system state to the current observation of the system.  $\mathbf{H}(n)$  contains the past system observations  $\mathbf{Y}(n) = (y^T(n-1), y^T(n-2) \dots y^T(n-p))$ :

	$\mathbf{H}(n) = \mathbf{I}_s \otimes \mathbf{Y}(n) = \begin{pmatrix} \mathbf{Y}(n) & 0 & 0 \\ 0 & \ddots & 0 \\ 0 & 0 & \mathbf{Y}(n) \end{pmatrix}$	6
--	---	---

where  $\otimes$  denotes the Kronecker product of matrices.  $\mathbf{v}_2(n)$  represents the measurement noise,  $\mathbf{v}_2(n) = N(\mathbf{0}, \mathbf{Q}_2(n))$ .

The state vector  $\mathbf{x}(n)$  can be estimated using the Kalman recursion. Modelling state transitions as a white-noise process (random walk) with a diagonal system noise covariance matrix  $\mathbf{Q}_1(n)$  leads to a simplified representation of the Kalman filter equations:

	$\begin{aligned} \mathbf{e}(n) &= \mathbf{y}(n) - \mathbf{H}(n) \hat{\mathbf{x}}(n n-1) \\ \mathbf{R}(n) &= \mathbf{H}(n) \mathbf{K}(n, n-1) \mathbf{H}^T(n) + \mathbf{Q}_2(n) \\ \mathbf{G}(n) &= \mathbf{K}(n, n-1) \mathbf{H}^T(n) \mathbf{R}^{-1}(n) \\ \hat{\mathbf{x}}(n+1 n) &= \hat{\mathbf{x}}(n n-1) + \mathbf{G}(n) \mathbf{e}(n) \\ \mathbf{K}(n, n) &= \mathbf{K}(n, n-1) - \mathbf{G}(n) \mathbf{H}(n) \mathbf{K}(n, n-1) \\ \mathbf{K}(n+1, n) &= \mathbf{K}(n, n) + \mathbf{Q}_1(n). \end{aligned}$	7
--	---	---

Here,  $\hat{\mathbf{x}}$  denotes the estimate of the true system state  $\mathbf{x}$ ,  $\mathbf{R}(n) = E[\mathbf{e}(n) \mathbf{e}^T(n)]$  is the one-step prediction error covariance matrix,  $\mathbf{K}(n, n)$  is the *a-posteriori* (filtered) state error covariance matrix, and  $\mathbf{G}(n)$  is the Kalman gain matrix, which in effect weighs the information in the measurements against the *a priori* knowledge of the system state.

When applying the Kalman algorithm to real data, the structure and update processes of the  $\mathbf{Q}_1$  and  $\mathbf{Q}_2$  covariance matrices are not known. Previous work has evaluated various  $\mathbf{Q}_1$  and  $\mathbf{Q}_2$  estimates under different noise statistics assumptions (Kasess 2002; Schlögl 2000).

Here, we define the AR model m1 by the following two noise covariance equations:

	$\mathbf{Q}_1(n) = \mathbf{I}_L UC$	8
--	-------------------------------------	---

where  $L = s^2 \times p$ , and

	$\mathbf{Q}_2(n) = (1 - UC) \mathbf{Q}_2(n-1) + UC \mathbf{e}(n) \mathbf{e}^T(n)$	9
--	---	---

where  $UC$  is the update coefficient ( $0 < UC < 1$ ) encoding the speed of adaptation of the AR model. The m1 model (Arnold et al. 1998) was shown to generate reliable estimates for various time-series data types and suggested to

perform better than several adaptive and segmentation-based AR models. The performance of m1 was robust when compared with several Kalman-filter implementations using alternative  $\mathbf{Q}_1$  and  $\mathbf{Q}_2$  formulations (Kasess 2002). In addition, several successful applications of m1 in modeling seizure propagation have been reported (van Mierlo et al. 2011, 2013; Wilke et al. 2008).

In the multivariate case, a more stringent assumption is that the measurement noise is instantaneously uncorrelated across time-series (Kasess 2002). That is, for  $i, j$  time-series, the zero-lag measurement noise cross-correlation  $corr_{i,j}(n, 0) = E(v_{2i}(n)v_{2j}(n))$  and its normalization with zero-lag auto-correlation values for  $i, j$  ( $Z_{i,j}(n, 0)$ ) are negligible:

	$Z_{i,j}(n, 0) = corr_{i,j}(n, 0) / \sqrt{corr_{i,i}(n, 0) corr_{j,j}(n, 0)} \cong 0$	10
--	---	----

In this case, off-diagonal elements of  $\mathbf{Q}_2(n)$  can be ignored, and the measurement noise update equation becomes:

	$\mathbf{Q}_2(n) = (1 - UC)\mathbf{Q}_2(n - 1) + UC\text{diag}(\text{diag}(\mathbf{e}(n)\mathbf{e}^T(n)))$	11
--	--	----

Here, equations 8, 11 define the AR model m2. Since  $\mathbf{Q}_2(n)$  is diagonal

	$\mathbf{Q}_2(n) = \begin{pmatrix} q_{21}(n) & & 0 \\ & \ddots & \\ 0 & & q_{2s}(n) \end{pmatrix}$	12
--	--	----

and the initial values of the state error covariance matrix  $\mathbf{K}$  are assumed to be diagonal or block diagonal

	$\mathbf{K}(1,0) = \begin{pmatrix} \mathbf{K}_1(1) & & 0 \\ & \ddots & \\ 0 & & \mathbf{K}_s(1) \end{pmatrix}$	13
--	--	----

Kalman equations can be separated into  $i = 1 \dots s$  distinct Kalman filters

	$\begin{aligned} e_i(n) &= y_i(n) - \mathbf{Y}(n)\hat{\mathbf{x}}_i(n n-1) \\ r_i(n) &= \mathbf{Y}(n)\mathbf{K}_i(n, n-1)\mathbf{Y}^T(n) + q_{2i}(n) \\ \mathbf{g}_i(n) &= \mathbf{K}_i(n, n-1)\mathbf{Y}^T(n)r_i^{-1}(n) \\ \hat{\mathbf{x}}_i(n+1 n) &= \hat{\mathbf{x}}_i(n n-1) + \mathbf{g}_i(n)e_i(n) \\ \mathbf{K}_i(n, n) &= \mathbf{K}_i(n, n-1) - \mathbf{g}_i(n)\mathbf{Y}(n)\mathbf{K}_i(n, n-1) \\ \mathbf{K}_i(n+1, n) &= \mathbf{K}_i(n, n) + \mathbf{Q}_{1i}(n). \end{aligned}$	14
--	---	----

As such, model m2 offers significant computational advantages, in part due to matrix size operations reduced by the order of  $s$ . At the same time, it is expected that the model m1 models highly correlated time-series more accurately.

### Time-varying functional connectivity

In order to evaluate the causal information flow between time-series, the signal represented by the AR coefficients can be used to derive Granger-causality measures of connectivity. To estimate functional connections in the frequency-domain, the Fourier transform of AR coefficients is first applied, as follows:

	$\mathbf{e}_f(f) = \mathbf{A}_f(f)\mathbf{y}_f(f)$	15
--	--	----

where

	$\mathbf{A}_f(f, n) = - \sum_{k=0}^p \mathbf{A}_k(n) e^{-i2\pi f k}$	16
--	--	----

$\mathbf{e}_f$ ,  $\mathbf{y}_f$  and  $\mathbf{A}_f$  are spectral transforms of the residuals, measured signal and AR coefficient matrices, respectively and  $\mathbf{A}_0(n)$  is the  $s$  times  $s$  identity matrix.

Within the class of frequency-based connectivity measures, the partial directed coherence (PDC, Baccala and Sameshima 2001) has been extensively used to model causal information flow in multivariate time-series. Both time-invariant and adaptive PDC representations have been applied to EEG-recorded seizures in order to characterize the seizures-onset regions and map the epileptic networks (Moeller et al. 2013; Omidvarnia et al. 2011; Varotto et al. 2010, 2012). PDC estimates the direct connections between time-series and their generators from indirect, or cascade, flows, within a functional network (Astolfi et al. 2008; Baccala and Sameshima 2001; Blinowska 2011). These connections are also directed, expressing the information flow between channels in source-sink terms. The adaptive PDC formulation used here, the integrated APDC (iAPDC), estimates the spectral information from channel  $j$  to channel  $i$  as follows:

	$iAPDC_{j \rightarrow i}(n) = \frac{1}{f_2 - f_1} \sum_{f=f_1}^{f_2} \frac{ A_{ij}(f, n) ^2}{\sum_{k=1}^s  A_{ki}(f, n) ^2}$	17
--	--	----

iAPDC is similar to squared PDC (Astolfi et al. 2006) integrated over a range of frequencies of interest ( $f_1:f_2$ ), which has proven to lead to robust connectivity estimates when compared with PDC (Astolfi et al. 2006, 2007; Florin et al. 2011). Here, iAPDC is used to evaluate the ability of m1 and m2 to model simulated iEEG seizures in the presence of noise with various cross-correlation structures.

### Simulations

30-sec, 10-channel seizure epochs were generated at a sampling frequency of 250 Hz. Each epoch consisted of baseline or background activity modeled as  $1/f$  multivariate random noise, and a seizure signal modeled as a sinusoid with a frequency evolving from 12 Hz at the seizure onset to 8 Hz at the seizure end (van Mierlo et al. 2011). The seizure began after a 10-sec pre-seizure baseline, and propagated successively from one channel to a maximum of three other channels chosen randomly for a total of 6 ‘ictal’ channels, after a delay between channels varying from 4 to 16 msec and a sample or phase delay of 4 to 12 msec. The sinusoidal signal was added to the background noise at a signal-to-noise ratio (SNR) of -5, 0, or 5 dB. SNR was defined as

	$SNR = 10 \log_{10} P_{signal}/P_{noise}$	17
--	---	----

With  $P_{signal}$  and  $P_{noise}$  the power of the sinusoid and the  $1/f$  noise, respectively.

An example of a simulated seizure and its corresponding network graph is shown in Fig. 1.

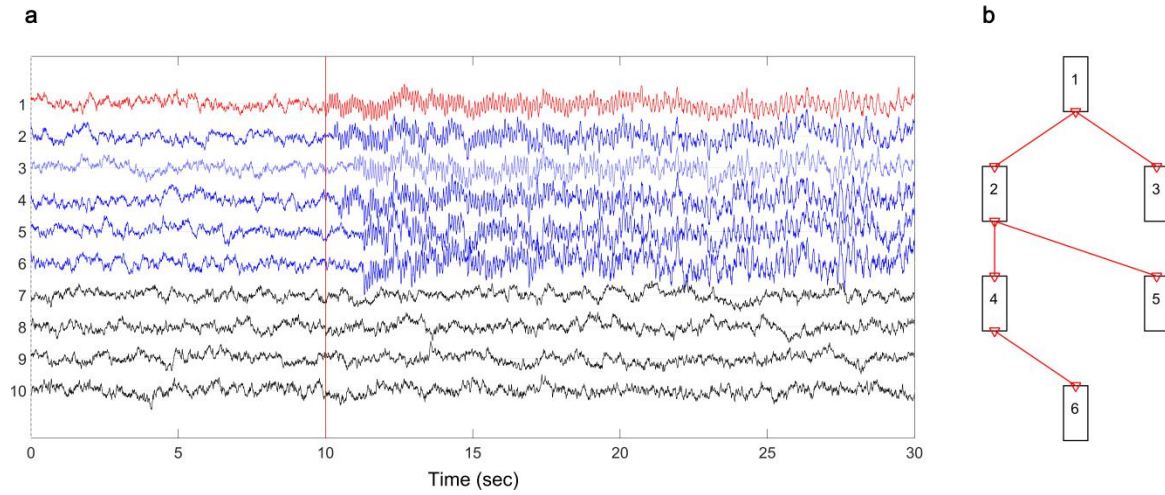


**Fig. 1** Simulated seizure. a. iEEG seizure epoch consisting of a 10-sec baseline prior to the seizure onset (vertical red line) in channel 1 (red) and spread to ictal channels 2-6 (blue); b. connectivity graph depicting the direct connections between ictal channels during the seizure

Several measurement-noise correlation structures were used to generate random, fully correlated, and focally correlated noise types. To this end, the noise covariance matrix entries for the  $(i,j)$  channel pairs were controlled using the normalized cross-correlation index  $Z_{i,j}$ . Random noise allowed only momentary instantaneous (zero-lag) correlations among times-series, thereby it was decorrelated over time (expected  $\sum_{n_1}^n Z_{ij}(n,0) = 0$  for all  $i,j$  pairs and  $n_t$  observations). Fully correlated noise, i.e. identical noise time-series, was obtained by setting  $Z_{i,j}(n,0)$  to 1 for all  $(i,j)$  at each time point. Focally correlated noise was generated by setting  $Z_{i,j}(n,0)$  to 1 for three and five channel pairs  $(i,j)$  at all  $t$  time points, corresponding to instances when up to half of all channels/ time-series are fully cross-correlated over time. These limit noise structures allow a ‘stress test’ of the ability of the m1 and m2 models to estimate the seizure signal connections modeled by the AR coefficients and iAPDC, and by extension, the direct connections characterizing the seizure network.

Combining the 3 SNR values and the 4 noise types resulted in 12 seizure epoch groups. For each group we performed 50 simulations. Within a group, each epoch was characterized by a unique noise time-series created with a random number generator. In addition, seizure epochs grouped based on focally correlated noise contained distinct channel pair combinations with identical noise time-series chosen randomly from the range of possible spatial configurations of such combinations within the seizure connectivity matrix.

### AR model evaluation based on simulations

The functional-connectivity profiles of the seizures in each of the 12 seizure groups were estimated with the m1 and m2 AR models in combination with iAPDC. Models m1 and m2 were applied to z-scored seizure time-series using a model order  $p$  of 5, and an update coefficient  $UC$  of  $10^{-4}$  selected by minimizing a model error index (REV, Schlögl 2000). The iAPDC values were calculated for a frequency window ranging from 2 to 50 Hz with frequency resolution equal to 0.1Hz. The analysis resulted in 24 connectivity data groups containing m1- and m2-derived connectivity matrices. Next, these matrices were thresholded in order to separate significant connections from noise and recover the functional networks of interest.

Selecting the optimal threshold is problematic when analyzing real data of unknown structure (Wang et al. 2014). With simulated data, the designed signal connections (Fig. 1b) constitute the ground truth against which various connectivity estimates can be evaluated and compared. Here, for each seizure, the network imposed by the propagated seizure signal served as the ground truth. In turn, this was used to calculate the number of false-positive and false-negative direct connections present in the m1- and m2-based connectivity matrices as a function of threshold. A receiver operating characteristic (ROC) curve was built for each connectivity matrix by varying the applied threshold from 0 to 1 in 0.01 steps, and the corresponding area under the curve (AUC) was calculated. The larger the AUC, the better an AR model was considered in identifying the underlying connectivity structure of the simulated seizure. Here, AUC values were adjusted so that  $AUC=1$  in case a threshold existed for which a model identified the ground-truth network of a simulated seizure (Wang et al. 2014). To assess the relative performance of the m1 and m2 AR models, the mean AUC values were first compared among connectivity data groups with repeated-measures analysis of variance (rANOVA). Between-group comparisons were then performed by applying the Tukey-Kramer correction for multiple testing at a significance level of 0.05.

### Realistic data

A 113-channel iEEG seizure epoch was analyzed from a patient who had undergone a right frontoparietal resection at the University of Texas Health Science Center at San Antonio. The substrate of his epilepsy consisted of an MRI-positive focal cortical dysplasia type IIb (Blümcke et al. 2011). The patient had been seizure free at the last clinic follow-up three years postoperatively. iEEG was recorded with subdural grids and strips at a 500-Hz sampling frequency, and contained 5-sec pre-seizure and 30-sec seizure segments identified by visual inspection of a clinical electroencephalographer (OL). The implantation scheme is depicted in Fig. 2. An 8x8-contact inferior frontal grid (IFG, interelectrode distance: 5 mm) overlay the lesion in the right perisylvian areas. An additional 2x5 superior frontal grid (interelectrode distance: 1 cm) and multiple strips were placed around IFG and interhemispherically. A 2-contact recording reference was placed over the anterior portion of the right superior frontal gyrus, removed from areas of high cortical irritability.

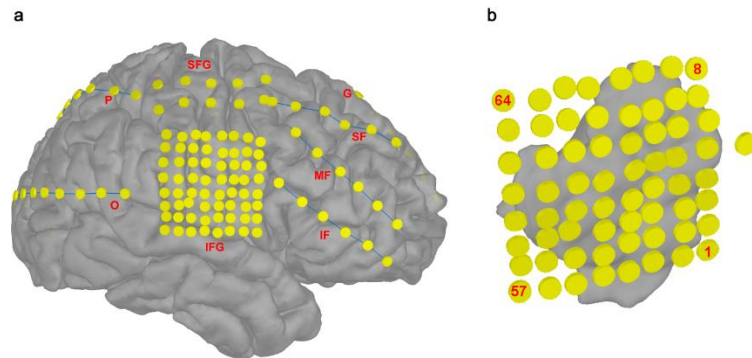


**Fig. 2** Intracranial electrode configuration. a. grid and strip electrodes overlying the lateral right hemisphere cortex; b. IFG contacts in relation to the reconstructed resection volume; G- ground, IF- inferior frontal strip, IFG- inferior frontal grid, MF- middle frontal strip, O- occipital strip, P- parietal strip, SF- superior frontal strip, SFG- superior frontal grid

Two seizure datasets were generated to examine whether using a large number of unselected channels in connectivity estimates of the epileptic network is feasible. First, a dataset comprised the 50 channels with the most prominent involvement in the electrographic seizure discharge based on visual analysis of the tracings. This reduced dataset was presumed to contain the seizure signal at a relatively high SNR. Second, a dataset consisting of all 113 time-series was selected. Next, the m1 and m2 AR models were applied to the z-scored 50-channel dataset. The 113-channel seizure was analyzed with the m2 model exclusively, because the memory cost associated with m1

application would be prohibitive (see Computational cost section below). The AR parameters used to calculate iAPDC estimates and the frequency band of interest were similar to the ones tested with simulated data. iAPDC values calculated for the 50-channel and 113-channel seizure datasets were then thresholded at the 95% percentile of a range of iAPDC values modelling the corresponding channel subsets of a carefully chosen 55-sec baseline iEEG segment (van Mierlo et al. 2011, 2013). This study was approved by the local institutional ethics research board.

#### AR model evaluation based on realistic data

While there is no ground-truth network graph for real datasets, in the case of seizures, the ability of a functional connectivity method to identify the channels driving the seizure, i.e. map the seizure onset, can inform of the method's ability to estimate correctly the causal information flow among time-series. As such, localizing the onset of a seizure to the resection volume in a patient free of seizures after surgery is supportive of a method's mapping accuracy.

In this study, the number of outgoing direct connections based on the matrix of thresholded iAPDC values from a channel or node to all other nodes was calculated at each time point, in order to estimate the prominence of that node within the seizure network. This number represents the outdegree, a graph theoretical measure expressed as

	$\phi_j(n) = \sum_{k=1}^S C_{kj}(n) \text{ iAPDC}_{kj}(n)$	18
--	--	----

where  $C_{kj}(n) = 1$  if  $\text{iAPDC}_{kj}(n)$  is at or above the threshold applied, and  $C_{kj}(n) = 0$  otherwise (van Mierlo et al. 2013). The channels with an outdegree value equal to or larger than 50% of the highest outdegree at each time point (i.e. full-width at half maximum, FWHM) were determined. These channels were thought to capture the majority of the information transfer during the seizures (i.e. 'ictal' channels) at that instant of time. Next, the resection volume was reconstructed as in Lie et al. (2015), and the electrode channels colocalizing with the resection were determined. The seizure-onset mapping accuracy was estimated by the degree of overlap over time between the collection of ictal channels and the contacts within the resection volume. This analysis was applied to both the m1 and m2-derived iAPDC estimates synthesized as outdegree values. In addition, the dynamic correlation between the outdegree-over-time maps resulting from the application of m1 and m2 models (50-channel dataset), and between the restricted and full datasets processed with m2, were estimated with the Pearson correlation coefficient. Briefly, a sliding time-window approach was used, with step/window lengths of 0.002 sec/0.002 sec (one time sample) and 0.25 sec/0.5 sec (Leonardi and Van De Ville 2015). For each time window, mean channel-specific outdegree values were ranked, transformed to normal scores and compared between datasets with the Pearson correlation coefficient (Bishara and Hittner 2012).

#### Computational cost

The memory and time costs of modeling times-series with m1 and m2 using graphics processing unit (GPU)-optimized code in MATLAB were estimated on 1-sec iEEG epochs of progressively larger datasets (16-192 channels) on a workstation PC with an 8-core Intel Xeon Processor E5-2667 v3 and a NVIDIA Quadro K6000 GPU with 12 GB memory.

### RESULTS

#### Simulated data

The relative performance of the m1 and m2 AR models when estimating direct connectedness in simulated networks with known structures was assessed using a workflow exemplified in Fig. 3.



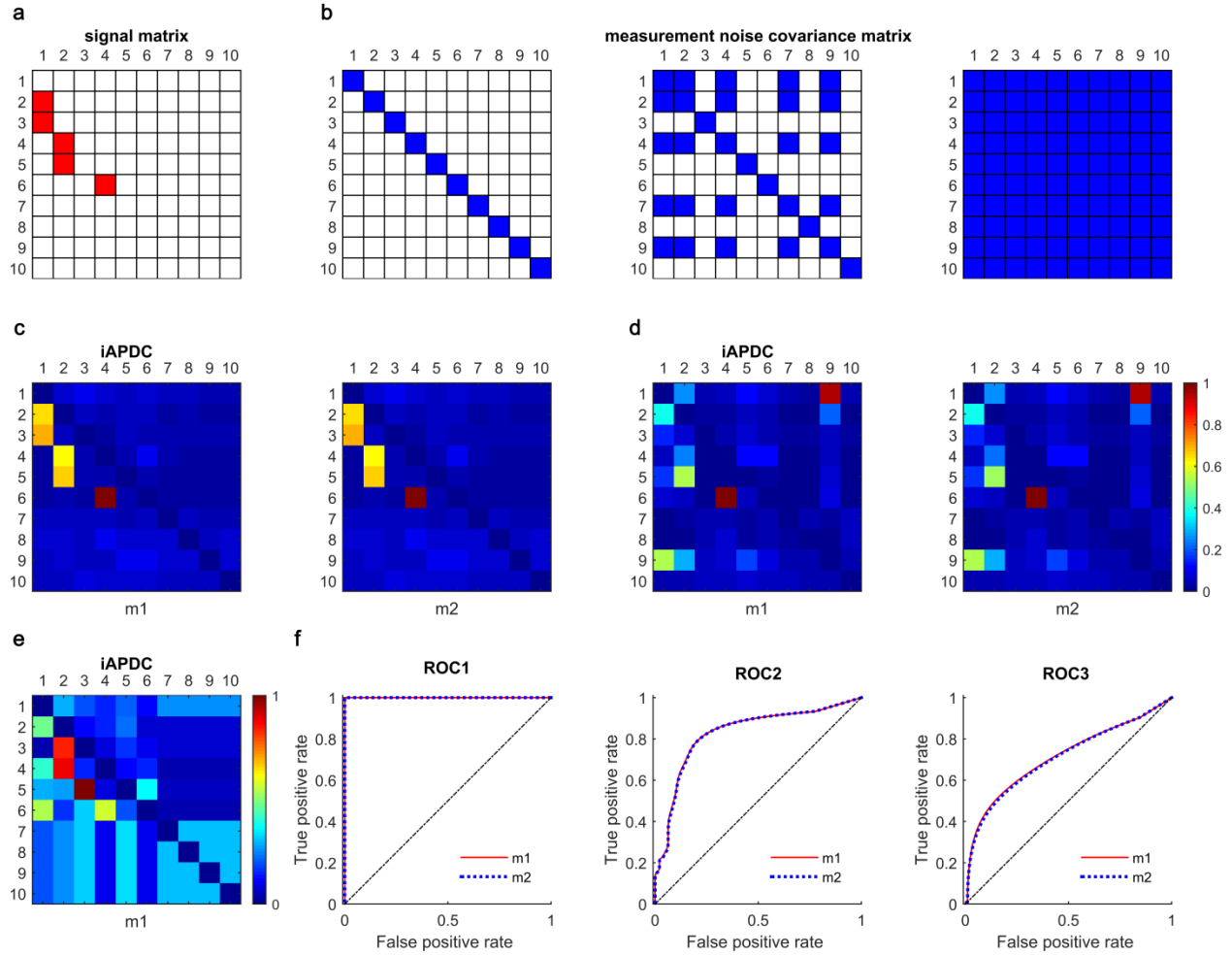


**Fig. 3** Functional connectivity analysis steps using the m1 and m2 AR models. a. The designed signal connectivity matrix of a seizure sinusoid encoding direct connections (red) formed during seizure propagation; b. Examples of measurement-noise structures, including random noise with a diagonal noise covariance matrix (left) with small-value off-diagonal elements (white) reflecting negligible cross-correlation between channels, focally correlated noise (blue) for five channel pairs (middle), and fully correlated noise (right); c, d, e. Time-averaged iAPDC connectivity matrices derived with m1 or m2 for individual seizures designed using signal and noise structures depicted in a and b, respectively. Here, added noise was random noise (c), focally correlated noise in five channel pairs (d), and fully correlated noise (e, m1 results shown) at SNR=0 dB; f. ROC plots corresponding to connectivity matrices in c (left), d (middle), and e (right)

In addition to the SNR used, seizure simulations differed based on their noise structure. The mean (standard deviation, stdev) values of the correlation index  $Z$  were 0.002 (0.01) for the pooled random noise structures, 0.06 (0.01) and 0.22 (0.02) for the focally correlated noise (three and five channel pairs, respectively), and 1(0) for the fully correlated noise.  $rANOVA$  of the AUC values resulting from ROC analyses used the AR model type as within-subject factor (Fig. 4). Statically significant differences between the m1 and m2 model performance were obtained for the noise type used,  $F(3, 588) = 112.30$ ,  $p_{value} < 0.001$ , and for a combined SNR-noise variable,  $F(11, 588) = 31.02$ ,  $p_{value} < 0.001$ . In the latter case, between-group comparisons disclosed small, yet statistically significant differences between m1- and m2-derived mean AUC values for seizure groups containing fully correlated noise (Fig. 4).

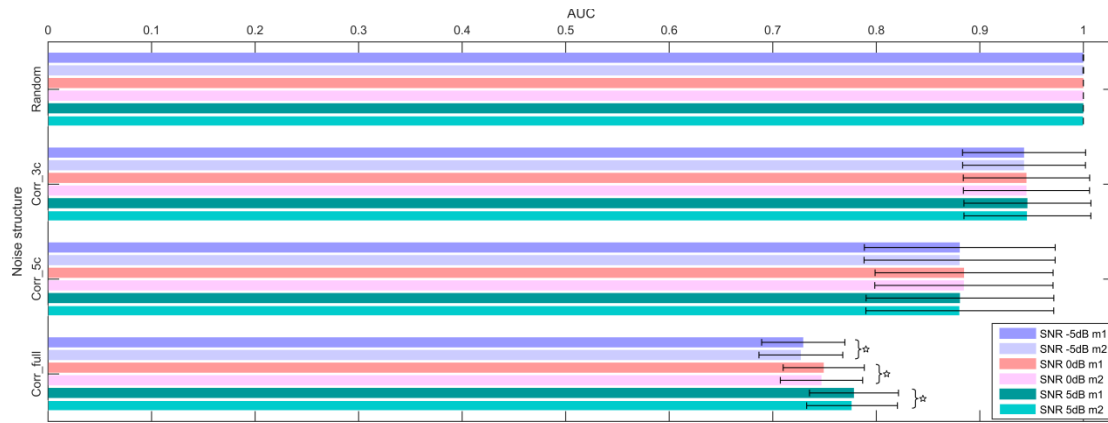


**Fig. 4** Comparison of mean AUC values among seizure groups analyzed with m1 and m2. Corr\_3c, Corr\_5c and Corr\_full label three-channel pair, five-channel pair, and fully correlated noise structures, respectively. Error bars represent AUC stdev for the respective groups. <sup>\*</sup>  $p_{value} < 0.001$  (Tukey-Kramer *post-hoc* test)

### Realistic data

The seizure onset was mapped by estimating the dynamic changes in the strength of direct functional connections encoded by the outdegree, for channel datasets processed with m1 (50 channels) and m2 (50 and 113 channels) in conjunction with iAPDC (Fig. 5). The channels driving the functional-connectivity outflow during the course of the seizure colocalized with the reconstructed resection volume for both m1 and m2 model analyses (Fig. 5a, b, c left). Channels IFG20, 29, 34, 35, 44, 45 were involved at the onset of the seizure for all datasets analyzed. Other ictal channels common to both the reduced and full iEEG datasets were identified only in the 50-channel data (IFG30) or the 113-channel data (IFG26, 38). There was a high degree of overlap between the seizure onset disclosed by m1 and m2 analyses and the resection volume, which was maximal at seizure onset and decreased during the course of the seizure as the ictal activity spread to other contacts (Fig. 5a, b, c right).

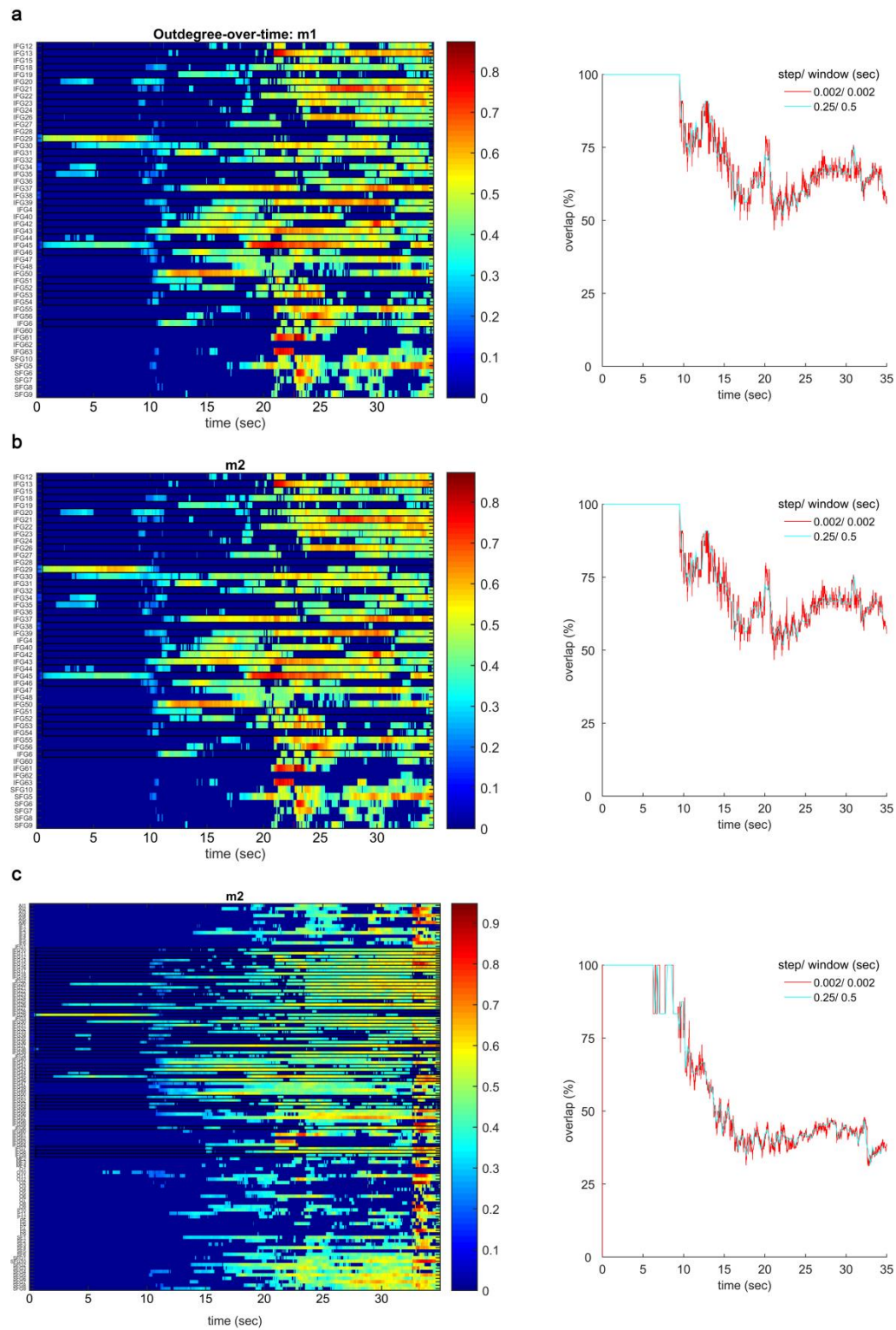


**Fig. 5** Colocalization of the seizure-onset estimates based on outdegree and the resection volume. Left: Outdegree-over-time maps obtained by thresholding channel-specific outdegree values for each time sample at 50% of the maximal outdegree at that point in time. a. m1/iAPDC, 50 channels; b. m2/iAPDC, 50 channels; c. m2/iAPDC, 113 channels. Boxed channels fall within the resection volume. Right: Sliding-window analyses of the degree of overlap between the resection volume and the channels with outdegree values above the threshold (see Left above)

Next, the correlation over time between outdegree estimates based on the two AR models (50-channel data) and for the restricted and full channel datasets (m2) was calculated. While the exact measurement-noise content in real electrographic seizure recordings is unknown, the baseline EEG can inform of the noise correlation structure when seen as the absence of a seizure ‘signal’. The mean correlation index  $Z$  calculated for the 55-sec iEEG baseline was 0.25 for the 50-channel dataset, and 0.19 for the 113-channel dataset. Outdegree value ranks were highly correlated over time, whether results from the two AR model analyses (50 channels) or m2-processed reduced and full channel data were compared (Fig. 6).

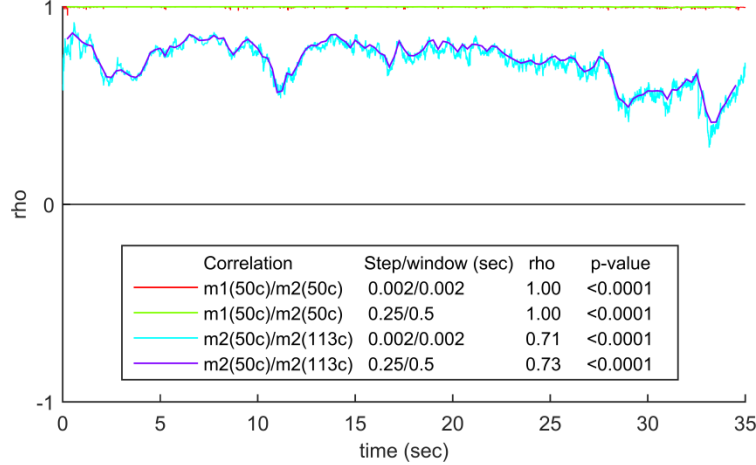


**Fig. 6** Dynamic correlation of the outdegree maps estimated based on m1 and m2. Time-matched Pearson correlation of the outdegree values resulting from m1 or m2 application. c- channel, rho- mean Pearson correlation coefficient

### Computational cost

The Kalman filter-based analysis is computationally expensive due to a rather large number of iterations, matrix operations, and matrix sizes. The current GPU code implementation of the m1AR model modifies the mvaar.m function from the BioSig library (Vidaurre et al. 2011) to reduce the run time of such analysis. m2 code replaces large 2D matrices with 3D arrays that shift the inputs of the  $s$  filters (equation 14) to the 3<sup>rd</sup> dimension, thereby reducing the size of filter-specific matrix operations (multiplication and inversion).

The memory cost of GPU-based operations is often limiting given the relatively small GPU memory sizes ( $\leq 24$  GB) of currently available units. In the case of m1, the memory cost per iteration is  $O(s^4 \times p^2)$ , representing the size of the state error covariance matrix  $\mathbf{K}$  (linear fit  $f(x) = 1.01s^4p^2 + 17.97$ , root-mean-square error 3.37), whereas for m2 it is  $O(s^3 \times p^2)$  ( $f(x) = 1.01s^3p^2 + 14.93$ , root-mean-square error 0.61). Table 1 lists the empirical memory and time costs attained when processing 1-sec iEEG segments with the m1 and m2 models using two model order values spanning a range commonly used in the literature:

AR model	Memory (MB)		Time (sec)	
	m1	m2	m1	m2
Model order: $p = 5$				
No. channels				
16	21	15	2.04	3.59
32	123	18	5.47	2.70
48	554	26	21.78	3.02
64	1714	42	81.30	3.52
96	8581	105	668.15	5.72
128	---	227	---	9.19
160	---	428	---	16.84
192	---	731	---	26.31

Model order: $p = 15$				
No. channels				
16	74	19	3.70	3.66
32	966	44	35.49	3.55
48	4821	115	227.11	5.76
64	---	253	---	9.84
96	---	821	---	26.90
128	---	1911	---	72.97
160	---	3714	---	164.36
192	---	6402	---	252.49

Table 1. Computational cost of AR analysis based on 1-sec iEEG epochs. --- out of memory

At this time, up to 100-channel time-series can be modeled with m1 (at low model order values). m2 accommodates high-density recordings of up to 192 channels, and is comparatively more time efficient ( $>100$  fold faster at high channel numbers). Fig. 7 displays functional connectivity estimates for a 30-sec simulated seizure recorded with 192 electrodes at 250 Hz, and processed with m2 ( $p = 5$ ) and iAPDC (frequency band 2:50 Hz). The analysis took 30 min to complete and was able to reconstitute the true network structure represented by designed signal matrix:

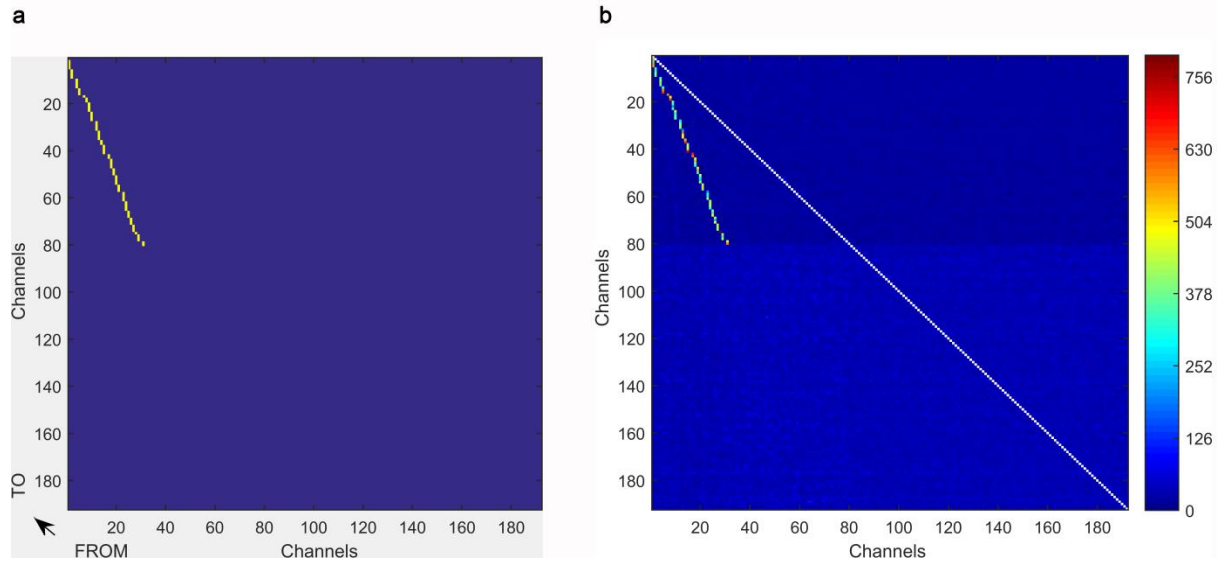


**Fig. 7** Functional-connectivity analysis of a seizure recorded with high-density iEEG. a. designed signal matrix for a seizure signal involving 80 ictal channels added to random background noise; b. iAPDC connectivity matrix of the seizure epoch obtained by summing up channel-pair-specific iAPDC values over time

## DISCUSSION

The main result of this study is that Kalman filter-based algorithms allow the estimation of dynamic functional connectivity for high-dimensional iEEG data. Here, GPU-accelerated implementations of m1, a well-studied random-walk vector AR model introduced by Arnold et al. (1998), and m2, a computationally efficient sequential derivation of m1, can process up to 100 and 192 time-series, respectively. Thereby, results support the possibility of routine large-scale, fully data-driven and quasi-automated multivariate dynamic connectivity analyses. The current approach ameliorates the hidden-source problem of iEEG recordings, obviating the need for time-series preselection before high-dimensional connectivity calculations are conducted. A more granular iEEG connectivity estimation may also facilitate cross-modality comparisons, especially when large-scale global connectivity studies using dense-array (scalp) EEG, magnetoencephalography, resting-state functional MRI, or diffusion-weighted imaging are planned. In addition, high-dimensional Kalman-based modeling has general applicability to data acquired with imaging techniques other than iEEG (Molenaar et al. 2016). These are all avenues to advance the view on how epileptic networks operate (Stufflebeam et al. 2011; van Dellen et al. 2009).

Whether including all available iEEG data for seizure-onset localization is beneficial in all cases needs further exploration. In practice, the number and location of electrode implants is determined based on more or less accurate localization hypotheses drawn noninvasively, and eloquent (i.e. functionally relevant) cortex mapping needs. In

addition, long-range functional changes at the scale of the fully sampled space have been noted during the seizures in both iEEG (Jiménez-Jiménez et al. 2015) and functional MRI (Englot et al. 2009) recordings. These changes may not reflect the seizure discharge proper or affect the seizure outcome after resective surgery (Jiménez-Jiménez et al. 2015) but may contribute significant connections in an analysis including a larger number of sampling contacts.

While such analysis may, in some cases, add ‘noise’ to localization estimates, it is independent of an often biased and laborious visual iEEG interpretation, in contrast to data preselection approaches. High-dimensional connectivity estimations may also change the relative connection weights for ‘signal-enriched’ time-series that would usually be preselected. As Fig. 5b, c (left) shows, the time-variant ranking of the outdegree values for several channels common to the reduced (50) and full (113) channel sets changed as a result of the number of channels analyzed. These mismatches increased during the evolution of the seizure, despite the otherwise high degree of correlation between the analyses of the two datasets (Fig. 6). Future studies including patients rendered seizure-free by surgery and those with continued seizures despite undergoing resection, will expand our understanding of the relative localization accuracy of high-density connectivity analysis.

Herein, a seizure-onset mapping method based on FWHM of outdegree values at each time point was inspired from similar approaches in source imaging using distributed inverse methods (Fuchs et al. 1999; Lie et al. 2015). The method needs further evaluation for its ability to identify the spatial extent of the seizure during its evolution, an important aspect when planning resection margins. In part, its performance depends of the choice of the threshold for the seizure connectivity matrix used to differentiate true connections from noise. Here, a computationally efficient method based on thresholds determined on a pre-seizure baseline was used (van Mierlo et al. 2011, 2013). Of the more computationally demanding surrogate statistics alternatives (Florin et al. 2011; He et al. 2011), thresholding based on random permutations uses a large number of AR model repetitions or runs to generate the distribution of a connectivity measure (e.g. iAPDC) under the null hypothesis. Since an individual run is processed efficiently on the GPU of a workstation PC with the present AR model coding strategy, the significant workload imposed by random permutations can be handled by the parallel distribution of runs to individual GPUs on a GPU supercomputer with fairly straightforward code adaptations. These thresholding techniques, and analytical approaches when available, merit further evaluation in simulation and realistic seizure studies.

Previously unreported, the analysis of simulated data suggests that the m1 AR model performs best in the presence of decorrelated noise. The m1 and m2 model accuracy decreases somewhat as the degree of noise correlation increases, with further modest reductions in m2 performance when the simulated noise is highly and globally cross-correlated (Fig. 4). Checking and correcting for correlated noise in real EEG recordings is problematic, because the artefactual and biological noise sources are difficult to separate, the boundaries between the seizure proper and seizure-related ictal electrographic changes are uncertain, and the presence of epileptiform patterns during baseline and volume conduction is confounding. One gross approximation of the ictal noise cross-correlation is to calculate the mean Z index on a baseline recording as done herein, assuming that the seizure epoch consists of a ‘seizure signal’ linearly added to noise with a correlation structure similar to that of the baseline used. A low Z value may increase the confidence in the estimated connectivity maps. Another approach is to compare the connectivity estimates for serial seizures in the same patient, among which the measurement noise correlation may vary. Since repeated seizures in individual patients often produce rather similar iEEG signals, they may be seen as realizations of the same stochastic process (Jouny et al. 2007; Korzeniewska et al. 2014). Finding conserved spatial motifs for the direct connections characterizing each of these seizures may improve seizure-onset mapping accuracy of the methods analyzed in this study. In addition, noise reduction techniques can be used to account for highly correlated noise. These include processing the raw recordings with methods such as independent-component analysis prior to the AR modelling step (Mullen et al. 2011), and excluding the frequency bands (main and harmonics) corresponding to the peak power of the line noise when conducting broadband frequency-domain connectivity estimations (Korzeniewska et al. 2014).

### **Future directions**

Several lines of research may be pursued to evaluate high-dimensional connectivity methods based on Kalman filtering in the context of epilepsy surgery. First, simulation studies are needed to extend the analysis of functional connectivity to the dynamic case for a range of direct (Baccalá et al. 2013; Korzeniewska et al. 2003) and indirect (van Mierlo et al. 2011, 2013) adaptive multivariate connectivity measures. Such tests can be conducted within a systematic framework using generative linear and nonlinear models, and various system and measurement noise types and frequency bands of interest (Wang et al. 2014). Second, comparative real-data studies of the degree of overlap between the estimated seizure networks, interictal epileptic and resting-state networks, and those revealed by controlled interventions such as cortico-cortical evoked potentials (Enatsu et al. 2012) may help better understand the process of ictal propagation in epilepsy. Third, any localization estimates based on dynamic functional connectivity need validation against seizure-altering treatments targeting network nodes focally. Colocalization of

the seizure connectivity maps (here; van Mierlo et al. 2013), or virtual resections derived from connectivity data (Sinha et al. 2014) with the actual resection volume reconstructions or electrical stimulation therapy (Morrell et al. 2011) contacts can be used to validate the connectivity-based methods when considering the postoperative (or post-stimulation) seizure control in individual patients (Brodbeck et al. 2011).

Steps such as these will help assessing the potential for integration of high-density connectivity analysis methods based on Kalman filter AR models into the formal presurgical evaluation of epilepsy surgery candidates.

Conflict of Interest: The authors declare that they have no conflict of interest.

## REFERENCES

- Andrzejak RG, David O, Gnatkovsky V et al (2015) Localization of epileptogenic zone on pre-surgical intracranial EEG recordings: toward a validation of quantitative signal analysis approaches. *Brain Topogr.* 28:832-7
- Arnold M, Miltner WH, Witte H, Bauer R, Braun C (1998) Adaptive AR modeling of nonstationary time series by means of Kalman filtering. *IEEE Trans Biomed Eng.* 45:553-62
- Astolfi L, Cincotti F, Mattia D et al (2007) Comparison of different cortical connectivity estimators for high-resolution EEG recordings. *Hum Brain Mapp.* 28:143-57
- Astolfi L, Cincotti F, Mattia D et al (2006) Assessing cortical functional connectivity by partial directed coherence: simulations and application to real data. *IEEE Trans Biomed Eng.* 53:1802-12
- Astolfi L, Cincotti F, Mattia D et al (2008) Tracking the time-varying cortical connectivity patterns by adaptive multivariate estimators. *IEEE Trans Biomed Eng.* 55:902-13
- Baccalá LA, de Brito CS, Takahashi DY, Sameshima K (2013) Unified asymptotic theory for all partial directed coherence forms. *Philos Trans A Math Phys Eng Sci.* 371:20120158
- Baccalá LA, Sameshima K (2001) Partial directed coherence: a new concept in neural structure determination. *Biol Cybern.* 84:463-74
- Bishara AJ, Hittner JB (2012) Testing the significance of a correlation with nonnormal data: comparison of Pearson, Spearman, transformation, and resampling approaches. *Psychol Methods.* 17:399-417
- Blinowska KJ (2011) Review of the methods of determination of directed connectivity from multichannel data. *Med Biol Eng Comput.* 49:521-9
- Blümcke I, Thom M, Aronica E et al (2011) The clinicopathologic spectrum of focal cortical dysplasias: a consensus classification proposed by an ad hoc Task Force of the ILAE Diagnostic Methods Commission. *Epilepsia.* 52:158-74
- Brodbeck V, Spinelli L, Lascano AM et al (2011) Electroencephalographic source imaging: a prospective study of 152 operated epileptic patients. *Brain.* 134:2887-97
- Bulacio JC, Jehi L, Wong C et al (2012) Long-term seizure outcome after resective surgery in patients evaluated with intracranial electrodes. *Epilepsia.* 53:1722-30
- Carrette E, Vonck K, De Herdt V et al (2010) Predictive factors for outcome of invasive video-EEG monitoring and subsequent resective surgery in patients with refractory epilepsy. *Clin Neurol Neurosurg.* 112:118-26
- Ding M, Bressler SL, Yang W, Liang H (2000) Short-window spectral analysis of cortical event-related potentials by adaptive multivariate autoregressive modeling: data preprocessing, model validation, and variability assessment. *Biol Cybern.* 83:35-45
- Enatsu R, Jin K, Elwan S, Kubota Y et al (2012) Correlations between ictal propagation and response to electrical cortical stimulation: a cortico-cortical evoked potential study. *Epilepsy Res.* 101:76-87
- Englot DJ, Modi B, Mishra AM, DeSalvo M, Hyder F, Blumenfeld H (2009) Cortical deactivation induced by subcortical network dysfunction in limbic seizures. *J Neurosci.* 29:13006-18
- Florin E, Gross J, Pfeifer J, Fink GR, Timmermann L (2011) Reliability of multivariate causality measures for neural data. *J Neurosci Methods.* 198:344-58
- Fuchs M, Wagner M, Köhler T, Wischmann HA (1999) Linear and nonlinear current density reconstructions. *J Clin Neurophysiol.* 16:267-95
- Granger, CWJ (1969) Investigating causal relations by econometric models and crossspectral methods. *Econometrica.* 37:424-438
- He B, Dai Y, Astolfi L, Babiloni F, Yuan H, Yang L (2011) eConnectome: A MATLAB toolbox for mapping and imaging of brain functional connectivity. *J Neurosci Methods.* 195:261-9
- Kalman RE (1960) A new approach to linear filtering and prediction theory. *Journal of Basic Engineering Trans. of ASME.* 82:34-45
- Kalman RE, Bucy RS (1961) New results on linear filtering and prediction theory. *Journal of Basic Engineering.* 83:95-108



Kasess CH (2002) Estimation of time-variant multivariate autoregressive models using Kalman filtering. Dissertation, Graz University of Technology

Korzeniewska A, Cervenka MC, Jouny CC et al (2014) Ictal propagation of high frequency activity is recapitulated in interictal recordings: effective connectivity of epileptogenic networks recorded with intracranial EEG. *Neuroimage*. 101:96-113

Korzeniewska A, Mańczak M, Kamiński M, Blinowska KJ, Kasicki S (2003) Determination of information flow direction among brain structures by a modified directed transfer function (dDTF) method. *J Neurosci Methods*. 125:195-207

Jiménez-Jiménez D, Nekkare R, Flores L et al (2015) Prognostic value of intracranial seizure onset patterns for surgical outcome of the treatment of epilepsy. *Clin Neurophysiol*. 126:257-67

Jouny CC, Adamolekun B, Franaszczuk PJ, Bergey GK (2007) Intrinsic ictal dynamics at the seizure focus: effects of secondary generalization revealed by complexity measures. *Epilepsia*. 48:297-304

Leonardi N, Van De Ville D (2015) On spurious and real fluctuations of dynamic functional connectivity during rest. *Neuroimage*. 104:430-6

Lie OV, Papanastassiou AM, Cavazos JE, Szabó ÁC (2015) Influence of intracranial electrode density and spatial configuration on interictal spike localization: a case study. *J Clin Neurophysiol*. 32:e30-40

Milde T, Leistriz L, Astolfi L et al (2010) A new Kalman filter approach for the estimation of high-dimensional time-variant multivariate AR models and its application in analysis of laser-evoked brain potentials. *Neuroimage*. 50:960-9

Moeller F, Muthuraman M, Stephani U, Deuschl G, Raethjen J, Siniatchkin M (2013) Representation and propagation of epileptic activity in absences and generalized photoparoxysmal responses. *Hum Brain Mapp*. 34:1896-909

Molenaar PC, Beltz AM, Gates KM, Wilson SJ (2016) State space modeling of time-varying contemporaneous and lagged relations in connectivity maps. *Neuroimage*. 125:791-802

Morrell MJ; RNS System in Epilepsy Study Group (2011) Responsive cortical stimulation for the treatment of medically intractable partial epilepsy. *Neurology*. 77:1295-304

Mullen T, Acar ZA, Worrell G, Makeig S (2011) Modeling cortical source dynamics and interactions during seizure. *Conf Proc IEEE Eng Med Biol Soc*. 2011:1411-4

Omidvarnia AH, Mesbah M, Khelif MS, O'Toole JM, Colditz PB, Boashash B (2011) Kalman filter-based time-varying cortical connectivity analysis of newborn EEG. *Conf Proc IEEE Eng Med Biol Soc*. 2011:1423-6

Rosenow F, Lüders H (2001) Presurgical evaluation of epilepsy. *Brain*. 124:1683-700

Schlögl A (2000) The electroencephalogram and the adaptive autoregressive model: theory and applications. Shaker Verlag, Aachen, Germany

Schlögl A, Supp G (2006) Analyzing event-related EEG data with multivariate autoregressive parameters. *Prog Brain Res*. 159:135-47

Sinha N, Dauwels J, Wang Y, Cash SS, Taylor PN (2014) An in silico approach for pre-surgical evaluation of an epileptic cortex. *Conf Proc IEEE Eng Med Biol Soc*. 2014:4884-7

Stufflebeam SM, Liu H, Sepulcre J, Tanaka N, Buckner RL, Madsen JR (2011) Localization of focal epileptic discharges using functional connectivity magnetic resonance imaging. *J Neurosurg*. 114:1693-7

Toppi J, Babiloni F, Vecchiato G et al (2012) Towards the time varying estimation of complex brain connectivity networks by means of a General Linear Kalman Filter approach. *Conf Proc IEEE Eng Med Biol Soc*. 2012:6192-5

van Dellen E, Douw L, Baayen JC et al (2009) Long-term effects of temporal lobe epilepsy on local neural networks: a graph theoretical analysis of corticography recordings. *PLoS One*. 4:e8081

van Mierlo P, Carrette E, Hallez H et al (2013) Ictal-onset localization through connectivity analysis of intracranial EEG signals in patients with refractory epilepsy. *Epilepsia*. 54:1409-18

van Mierlo P, Carrette E, Hallez H et al (2011) Accurate epileptogenic focus localization through time-variant functional connectivity analysis of intracranial electroencephalographic signals. *Neuroimage*. 56:1122-33

van Mierlo P, Papadopolou M, Carrette E et al (2014) Functional brain connectivity from EEG in epilepsy: seizure prediction and epileptogenic focus localization. *Prog Neurobiol*. 121:19-35

Varotto G, Franceschetti S, Spreafico R, Tassi L, Panzica F (2010) Partial directed coherence estimated on stereo-EEG signals in patients with Taylor's type focal cortical dysplasia. *Conf Proc IEEE Eng Med Biol Soc*. 2010:4646-9

Varotto G, Tassi L, Franceschetti S, Spreafico R, Panzica F (2012) Epileptogenic networks of type II focal cortical dysplasia: a stereo-EEG study. *Neuroimage*. 61:591-8

Vidaurre C, Sander TH, Schlögl A (2011) BioSig: the free and open source software library for biomedical signal processing. *Comput Intell Neurosci*. 2011:935364



Wang HE, Bénar CG, Quilichini PP, Friston KJ, Jirsa VK, Bernard C (2014) A systematic framework for functional connectivity measures. *Front Neurosci.* 8:405

Wilke C, Ding L, He B (2008) Estimation of time-varying connectivity patterns through the use of an adaptive directed transfer function. *IEEE Trans Biomed Eng.* 55:2557-64

Yaffe RB, Borger P, Megevand P et al (2015) Physiology of functional and effective networks in epilepsy. *Clin Neurophysiol.* 126:227-36